Appl. Phys. B 50, 247–256 (1990)

Applied Physics B Photophysics and Laser Chemistry

Observation of Gain at 54.2 Å on Balmer-Alpha Transition of Hydrogenic Sodium

Y. Kato[1], E. Miura[1], T. Tachi[1], H. Shiraga[1], H. Nishimura[1], H. Daido[1], M. Yamanaka[1], T. Jitsuno[1], M. Takagi[1], P. R. Herman[1]*, H. Takabe[1], S. Nakai[1], C. Yamanaka[1], M. H. Key[2], G. J. Tallents[2], S. J. Rose[2], and P. T. Rumsby[2]**

[1] Institute of Laser Engineering, Osaka University, Suita, Osaka, 565 Japan
[2] Rutherford Appleton Laboratory, Chilton, Didcot, Oxfordshire OX11 0QX, UK

Received 31 October 1989/Accepted 29 November 1989

Abstract. Planer stripe and foil targets coated with NaF were irradiated with high intensity 351 nm laser radiation of 130 ps duration. Time-integrated as well as time-resolved measurement of gain on NaXIHα at 54.2 Å were made. A time-integrated gain of $1.2^{+0.8}_{-1.1}\,\mathrm{cm}^{-1}$ and a time-resolved peak gain of $3.2 \pm 1.0\,\mathrm{cm}^{-1}$ were obtained. A detailed account of the experimental procedures for determination of gain is given.

PACS: 32.30.Rj, 42.55.Hq, 52.70.La

There has been rapid progress recently in the development of soft X-ray lasers by several approaches. Soft X-ray amplification was observed in a laser-produced plasma using an exploding foil target due to electron-collisional excitation [1] on neon-like Se (at 206 and 209 Å) [2] and other higher-Z ions [3], as well as on nickel-like ions of Eu at 71 Å [4] and Yb at 50 Å [5]. Using solid slab targets of Cu and Ge, amplification was also observed with this scheme at 200–300 Å [6]. Significant amplification on C VI Balmer-α(Hα) by recombination pumping was demonstrated with a magnetically-confined laser-produced plasma [7]. Recombination pumping of the Hα transition in hydrogenic ions due to rapid cooling by adiabatic expansion of fully stripped ions using thin fiber targets resulted in observation of gain [8] and demonstration of amplification [9] on C VI at 182 Å and F IX at 81 Å [10]. Thin foil targets were also used to observe gain on Hα of C VI [11, 12], O VIII [13], and F IX [14]. By recombination pumping of $5f$-$3d$ and/or $4f$-$3d$ transitions of Li-like Al, gain was observed using a solid target [15, 16], a thin fiber [10], a thin foil [14], or a magnetically-confined plasma [17].

One of the important objectives of the current research is to develop a soft X-ray laser useful for high-resolution holographic imaging of biological specimens. Recent theoretical study shows that the optimum laser wavelength for this application will be very close to, but slightly longer than the carbon K-edge at 43.7 Å [18]. With electron-collisional excitation, amplification at 50.3 Å was observed with Ni-like Yb [5], and theoretical evaluation for the Ni-like W laser at 43.1 Å has been reported [19].

Isoelectronic scaling of the recombination-pumped Hα laser to shorter wavelengths requires target irradiation with short wavelength and short pulse laser at high irradiation intensity. Guided by the scaling considerations which are described in the next section, we have performed an experiment on the Hα laser in order to observe amplification near and below 50 Å. Stripe targets were irradiated with a 351 nm, 130 ps laser pulse and evidence for gain on Na XI Hα at 54.2 Å and Mg XII Hα at 45.5 Å was obtained in time-integrated measurement [20]. On Na XI Hα, dependence of gain on target structure and target material was also studied. In addition time-development of gain on Na XI Hα was measured from streaked spectra [21]. In this paper we describe detailed experimental conditions and present the experimental results on determination of gain on Na XI Hα in time-integrated as well as time-resolved measurements.

* Present address: Department of Electrical Engineering, University of Toronto, Toronto, Ontario, Canada, M5S 1A4
** Present address: Institute for Laser Technology, Utsubo-honmachi, Nishi-ku, Osaka, 550 Japan

1. Isoelectronic Scaling of Recombination Balmer-α Laser

An extensive theoretical model for the recombination C VI Hα laser at 182 Å in rapidly expanding cylindrical plasmas has been developed by Pert [22–25]. By separately analyzing the initial burn for heating the plasma to fully-stripped ionic states and the following adiabatic expansion to produce gain, optimal conditions for the mass and the thermal energy of the heated plasma were determined. Once the reference conditions are determined for C VI Hα, this recombination scheme can be extended to shorter wavelengths by considering similarity forms for the collisional radiative rate equations for the hydrogenic ions of charge Z [26]. This leads to Z-dependence of the transition wavelength as $\lambda \sim Z^{-2}$, the electron temperature $T \sim Z^2$, the electron density $n_e \sim Z^7$, the time scale $t \sim Z^{-4}$, and the gain coefficient $g \sim Z^{7.5}$ for a Doppler-broadened line [22]. However these Z scalings have a limit at $Z \sim 12$ since the electron density cannot exceed the initial density of the solid material unless, for example, laser-driven compression is utilized [23]. Key [27] considered laser-intensity dependence of the temperature and density in initial formation of the plasma in laser-driven ablation, and shows that the initial electron temperature can be increased as $T_e \sim Z^2$ when the laser intensity is scaled as $I \sim Z^4$ but the initial electron density scales only as $n_e \sim Z$ due to the finite density that the laser light can penetrate. Starting from this initial plasma formation condition, the gain scales as $g \sim Z^{-1/2}$ instead of $g \sim Z^{7.5}$. Since the initial electron density is inversely proportional to the laser wavelength, a short wavelength laser for target irradiation favours higher gain.

On C VI Hα, a peak gain of $4\,\mathrm{cm}^{-1}$ was attained 1 ns after laser irradiation of 90 ps duration at the absorbed energy of 2.6 J/cm using a fiber of 7 μm diameter [9]. From the absorbed intensity of $1.7 \times 10^{13}\,\mathrm{W/cm^2}$ for this case, the absorbed intensity for Na XI Hα should be $2.7 \times 10^{14}\,\mathrm{W/cm^2}$ when we assume Z^4 scaling. A higher irradiation intensity might be required in order to keep the ionization fraction at a high level [28]. The laser pulse duration, which is required to be shorter than the time reaching to the maximum gain, should preferably be less than $1\,\mathrm{ns}/(6/11)^4 = 89\,\mathrm{ps}$. The expected peak gain is $g \sim 3\,\mathrm{cm}^{-1}$.

When the recombination laser is scaled to shorter wavelengths, rapid temperature decrease due to adiabatic expansion becomes less effective and other cooling mechanisms such as thermal conduction to colder region of the plasma and radiation cooling will become increasingly important. In this case a thin ribbon target [29] may be used alternative to a thin fiber target, since the former can couple better to laser light of finite focus width and its mass can be controlled by the width and thickness of the target. A stripe target where a stripe of laser material is coated on a thin plastic foil may perform equivalently to a ribbon target when the substrate foil thickness is sufficiently thin compared with the ablation depth. In the case of planar targets, which includes a foil target where the laser material is coated over the whole area of a thin foil, plasma expansion is close to planar in the initial expansion stage. Therefore adiabatic cooling will be less and L_α trapping will be stronger. Also heating of excess target material due to lateral thermal conduction may cause difficulty in gain observation due to increased spontaneous emission [30].

Trapping of Lyman-α radiation has been considered to be a major limitation to the Hα gain, and a diluted target was examined in which fraction of the lasing atoms is decreased to reduce L_α trapping, thereby increasing gain [30]. However recent detailed comparison of the F IX Hα laser with computer modeling shows that the trapping factor used in previous codes has probably overestimated the degree of self-absorption [31].

2. Experimental Conditions

A schematic of the target structures tested in this work is shown in Fig. 1. The fiber target was a 7 μm carbon fiber coated with NaF of 1 μm thickness. The stripe target was a 30 μm-wide and 1 μm-thick NaF coated on one side of a 0.13 μm-thick CH plastic foil. The foil target was a 0.2 μm-thick NaF coated over one surface of a 0.13 μm-thick CH plastic foil. A $Na_2B_4O_7$ stripe was also fabricated to test the dilution effect for Na. The width of the substrate foil along the length of the stripe was limited to 6 mm which was shorter than the line focus length of the irradiating laser beam. The stripe and the foil targets were irradiated with one beam from the coated side, whereas the fiber target was irradiated with two opposing laser beams.

The experiment was carried out on GEKKO XII neodymium glass laser facility at the Institute of Laser

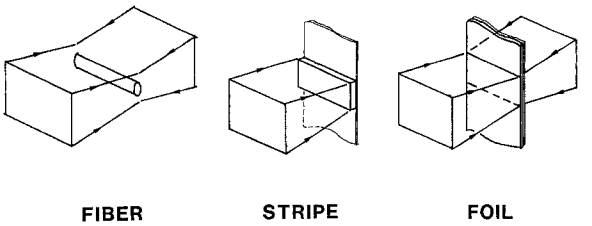

Fig. 1. Schematic drawings of the fiber, stripe, and foil targets tested in this work

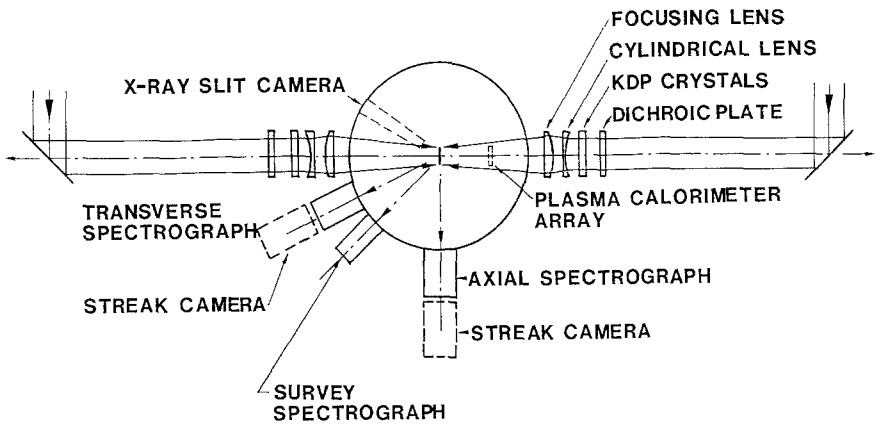

Fig. 2. Layout of the laser beams and the diagnostic equipment used in the present experiment. A set of two split-field imaging microscopes used for target alignment, not shown in this layout, was placed in the plane normal to the axis of the X-ray laser target

Engineering, Osaka University. Two of its 12 beams were used for this experiment in an optical layout shown in Fig. 2. Each laser beam of 1.053 μm wavelength and 32 cm beam diameter was frequency-tripled to 351 nm with two KDP crystals, each of which was composed of 4 segmented elements. Dichroic mirrors were added to protect the IR-reflecting turning mirrors from damage caused by transmitted UV light from the opposing laser beam when a fiber target was irradiated with two beams. A combination of a weak negative cylindrical lens and an $f/3$ 1 m aspheric lens produced 7 mm-long line focus on target. The line focus width is determined by the finite divergence of the laser beam since optical ray-trace calculation for this line focus optics shows negligible aberrations. The actual width measured from the time-integrated X-ray emission pattern was 50 μm in full-width at half-maximum intensity. The maximum UV laser energy on target was 152 J per beam at a pulse length of 130 ps, corresponding to the maximum intensity of 3.3×10^{14} W/cm^2. A shorter pulse duration was not available at the time of the experiment.

The experiment required precise alignment of the line-focused UV laser beam on a thin target such as a stripe or a fiber. A split-field imaging microscope system developed at the Rutherford Appleton Laboratory [32] was installed onto the vacuum chamber. Two split-field microscopes viewed the target from two orthogonal directions normal to the target axis. The split-field microscope system enabled precise target alignment with accuracies of 1 mrad in angle and 5 μm in space, although the transparent stripe target required careful alignment due to low contrast of the image. The reference position of the split-field microscopes were first determined by a thin metal wire which was extended straight between the centers of the two ports of the chamber located normal to the GEKKO XII laser beam axis. The axial spectrometer shown in Fig. 2 was aligned on the axis of the wire using an alignment telescope to ~1 mrad accuracy. Laser alignment on target was carried out first at IR by positioning a 30 μm-wide slit target using the split field microscope. Laser focusing and angular positioning of the cylindrical lens were adjusted by observing the GEKKO XII IR beam transmitted through the slit target using the alignment monitoring package placed behind the final turning mirror which viewed the magnified image of the target. The inverse Foucault pattern transmitted through the slit was also used to fine tune the angle of the line focus to the slit. Finally the lens was moved toward the target by a known amount (~6 cm) for UV focusing, and low energy (200 mJ) shots at 3ω were fired at a 10 μm thick copper target which had crossed-slit marks for positioning. Examination of the burn marks on the surface with an optical microscope gave accurate information on the positioning of the line focus. Accuracies of ±7 μm and ±1 mrad at 3ω were accomplished. The low energy shot on the copper target was made each day before the main target shots for precise laser irradiation on thin targets. The X-ray laser target was positioned carefully relative to the line focus so that the 6 mm length was completely covered by the 7 mm long line focus in order to avoid the edge effects.

Two XUV spectrometers, time-resolved with streak cameras, were used for spectroscopic diagnostics. Each of these spectrometers was equipped with a 3° grazing incidence spherical focusing mirror which formed a 10:1 reduced astigmatic image of the source onto the slit. Since both the spherical mirror and the spectrometer slit were horizontally positioned, the reduced image along the width of the line focusing was formed on the slit. The first spectrometer, aligned onto the target axis, had a 1200 lines/mm variable spacing diffraction grating for flat field recording of the spectra operated at 3.2° grazing angle [33]. With X-ray film recording, it gave spectra from 30Å to 370Å over a 5 cm field with a resolution of 0.2Å at around 50Å.

Using a Hamamatsu streak camera (Model C 2950) with a CuI photocathode [34], a 25 mm field was recorded with 0.5 Å resolution. The output image of the streak camera was monitored with an SIT tube and stored in a digital frame memory. The second spectrometer positioned 60° off-axis had a 2400 lines/mm variable spacing diffraction grating operated at 1.2° grazing angle. It gave photographic spectra in a 5 cm field from 6 Å to 150 Å with 0.1 Å resolution near 50 Å. A Kentech streak camera with a low density CsI photocathode recorded a 25 mm field with 0.3 Å resolution. The output image was recorded with a high sensitivity photographic film which was in close-contact to the fiber optic face plate of the image intensifier attached to the streak camera. Another spectrometer positioned 45° off-axis (Spectral Precision Model 1100-S with film recording) gave time-integrated XUV spectra over 8–200 Å on a Rowland circle which were used to evaluate the plasma conditions.

Time-integrated X-ray emission image of the target was recorded with an X-ray slit camera which was composed of two orthogonal slits to provide a higher magnification perpendicular to the line focus. An array of 12 plasma calorimeters was positioned to record narrow angular distribution of plasma energy perpendicular to the target axis.

3. Experimental Procedures for Gain Determination

The procedure for gain determination used in this experiment was to compare the intensities emitted along (I_a) and transverse (I_t) to the X-ray laser axis. Approximating the plasma as a long column of length L and area A, these intensities are given respectively by $I_a = I_{sp}A[\exp(gL)-1]/g$ and $I_t = I_{sp}AL$, where I_{sp} is the spontaneous emission intensity per unit volume. This is valid when the opacity along the transverse dimension is small. Since

$$I_a/I_t = [\exp(gL)-1]/(gL), \quad (1)$$

we can determine the gain-length product from I_a/I_t. This procedure enables us to determine gain or loss of various spectral lines in each shot.

In order for this procedure to be valid, the relative sensitivity of the two spectrometers has to be accurately calibrated. Calibration was made by recording time-integrated spectra of the XUV emission from a narrow (1 mm-wide) planer foil whose target normal was oriented at an angle bisecting the two spectrometers (inset in Fig. 3). Since the two spectrometers viewed the small plasma from symmetric directions, the relative sensitivity is determined irrespective of the optical thickness of the calibration spectral lines. Another requirement for the cross calibration is that the collection efficiency of the XUV emission from the target by each spectrometer has to be constant irrespective of the target length. This requirement was fulfilled by forming a 10:1 reduced image of the X-ray source onto a slit of each spectrometer which was wide opened to 500 μm width. In spite of the wide slit widths, good spectral resolution of ~0.1 Å (axial) or ~0.2 Å (transverse) was obtained confirming narrow and horizontal imaging of the X-ray source onto the entrance slits. The narrow foil used for cross calibration was coated with $Na_2B_4O_7$ which provided strong calibration lines over 40–71 Å which are listed in Table 1. The calibration data were taken at the beginning and end of the measurements on

Table 1. Calibration lines used to determine the relative sensitivity of the axial and transverse spectrometers

Transition		Wavelength [Å]
C V	$2p^1P^0{}_1$–$1s^1S_0$	40.268
B V	$2p^2P^0{}_{3/2}$–$1s^2S_{1/2}$	48.586
B V	$2p^2P^0{}_{1/2}$–$1s^2S_{1/2}$	48.591
Na IX	$4d^2D_{3/2}$–$2p^2P^0{}_{1/2}$	58.201
Na IX	$4d^2D_{5/2}$–$2p^2P^0{}_{3/2}$	58.279
B IV	$2p^1P^0{}_1$–$1s^1S_0$	60.314
Na IX	$3p^2P^0{}_{3/2}$–$2s^2S_{1/2}$	70.615
Na IX	$3p^2P^0{}_{1/2}$–$2s^2S_{1/2}$	70.653

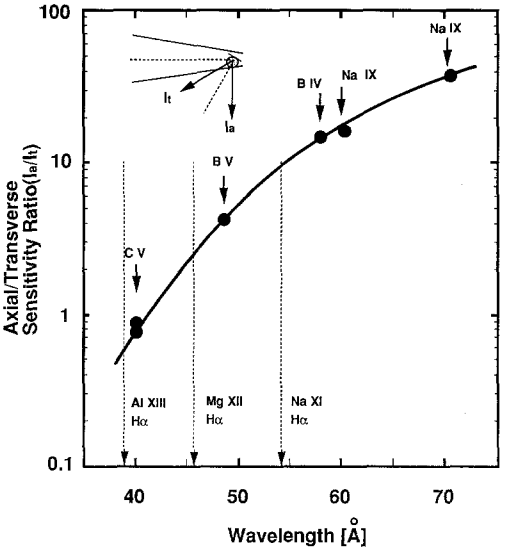

Fig. 3. Relative sensitivity of the axial and transverse spectrometers determined by irradiating a narrow stripe target coated with $Na_2B_4O_7$ in an arrangement shown in the inset. Wavelengths of the calibration lines and the Hα transitions of Na, Mg, and Al are indicated

Na to confirm the reproducibility. The relative sensitivity of the axial and transverse spectrometers plotted against the wavelength is shown in Fig. 3. Due to different spectral reflectivities of the gratings used in the two spectrometers, the sensitivity ratio depends strongly on the wavelength. However reliable measurement is possible over approximately 55–44Å where the sensitivity ratio varies from 10 to 1.

Time-integrated spectra were recorded with Kodak 101-07 film. Particular precautions were taken for handling this sensitive film to avoid background noises and to reduce the fog level. The characteristic response curve of the batch of the film used in this experiment was determined by recording spectra from laser-produced Al plasmas at different exposures which were controlled by placing stepped Al filters of known thicknesses at the entrance slit of the spectrometer. Although this film calibration method does not provide absolute scale to the exposure of the film, it is sufficient for the present purpose since only the spectral intensity ratio between the two instruments is required. The experimental data for the film density vs exposure is shown in Fig. 4. The data can be fitted well to the equation (given in the inset in Fig. 4) which is valid for a film coated with thin emulsion [35]. It should be noted that the constants ($c_1 \sim c_3$) depend on the batch of the film, and also on the numerical aperture of the densitometer. This curve is different from the Henke's data obtained with a cw X-ray source [36] and closer to the data obtained with a pulsed, laser-plasma X-ray source at the Max-Planck-Institut für Quantenoptik, Garching [37]. The error of the response curve

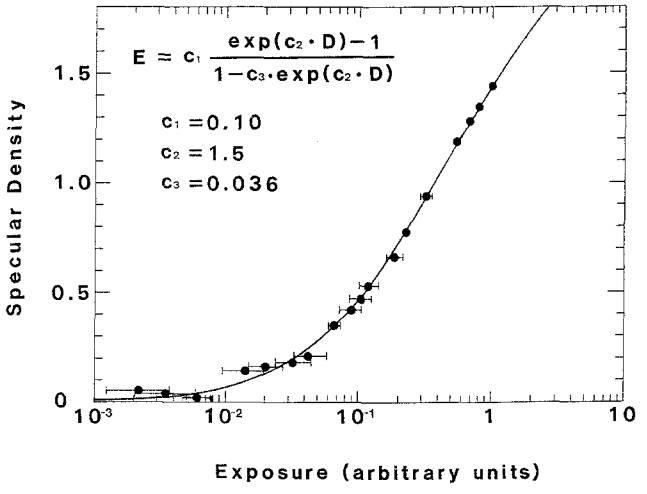

Fig. 4. Characteristic response curve of a Kodak 101 07 film used in this experiment, determined with a pulsed laser plasma X-ray source. The numerical aperture of the densitometer is 0.10. The exposure on the horizontal axis is in arbitrary units. The solid curve is the best fit to the experimental data by the equation given in the inset

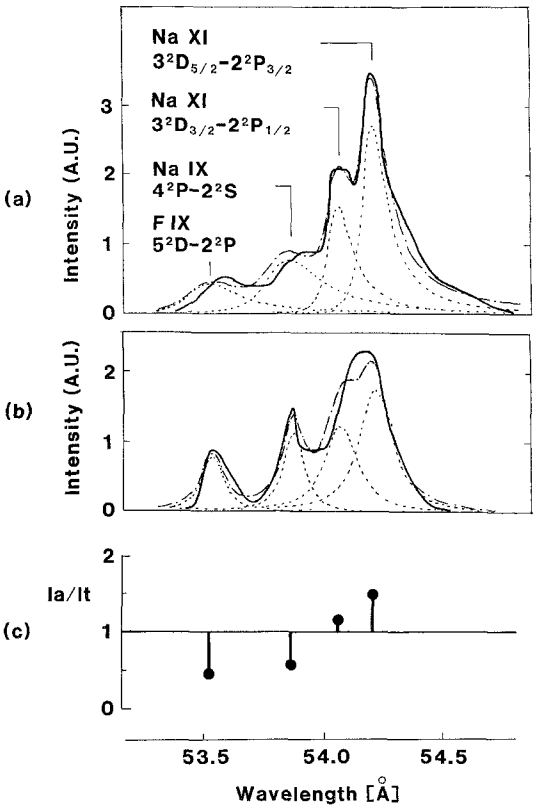

Fig. 5. The thick solid curves show observed spectral profiles at 53.3–54.7Å for (**a**) axial and (**b**) transverse spectra. The Na XI Hα $J=5/2$–$3/2$ and $J=3/2$–$1/2$ doublet are blended with Na IX $4p$–$2s$ and F IX $5d$–$2p$ lines. The thin dotted curves are the deconvoluted line shapes of these lines and thin line-dot curves are the convoluted line shapes. The axial-to-transverse intensity ratio for each line is shown in (**c**)

shown in Fig. 3, which arises mainly from the inaccuracy of the Al filter thickness, becomes smaller above $0.3\,D$ where most of the data were analyzed for cross calibration and gain determination.

High spectral resolution achieved by recording spectra with the film enabled us to resolve and accurately assign spectral lines, and to determine gain or loss of each line. Line shapes of the axial and transverse spectra of NaF near 54Å are shown by the thick solid curves in Fig. 5. These curves were obtained from the densitometer traces and using the film response curve shown in Fig. 4. The Na XI Hα is composed of a doublet structure, $J=5/2$–$3/2$ line at 54.194Å and $J=3/2$–$1/2$ line at 54.052Å, and is closely overlapped with Na IX $4p^2P$-$2s^2S$ at 53.860Å and slightly with F IX $5d^2D$-$2p^2P$ at 53.527Å. Although these lines are not clearly resolved in the spectra shown in Fig. 5, we can determine the relative intensities and evaluate mutual overlaps knowing the wavelengths of these lines and the spectral resolution curve of each spectrometer derived from nearby isolated spectral

lines. The thin dotted curves in Fig. 5 show the deconvoluted shapes of each line and the thin line-dot curves are the convolved line shapes. The agreement between the data and the convolved shape is less in Fig. 5b due to smaller intensity of the transverse spectrum. From this analysis, we can evaluate the overlaps of the nearby lines to the Hα $J=5/2$–$3/2$ line which should show the highest gain.

Time-resolved spectra were taken with the streak cameras as described in the previous section. The relative sensitivity of the two instruments with the streak cameras included was calibrated at 48.59 Å from the streak traces of the B V $2p^2P$–$1s^2S$ line emitted from a narrow calibration target which was irradiated in the same way as in the time-integrated calibration measurement. The relative sensitivity at 54.2 Å was then determined from the relative spectral response of the two spectrometers shown in Fig. 3 and from the published spectral sensitivity curves of the streak camera photocathodes. Linearity and dynamic range of the Hamamatsu streak camera with the SIT recording used for the axial spectrometer and the characteristic curve of the photographic film used for the Kentech streak camera attached to the transverse spectrometer were calibrated, respectivity, in an independent measurement.

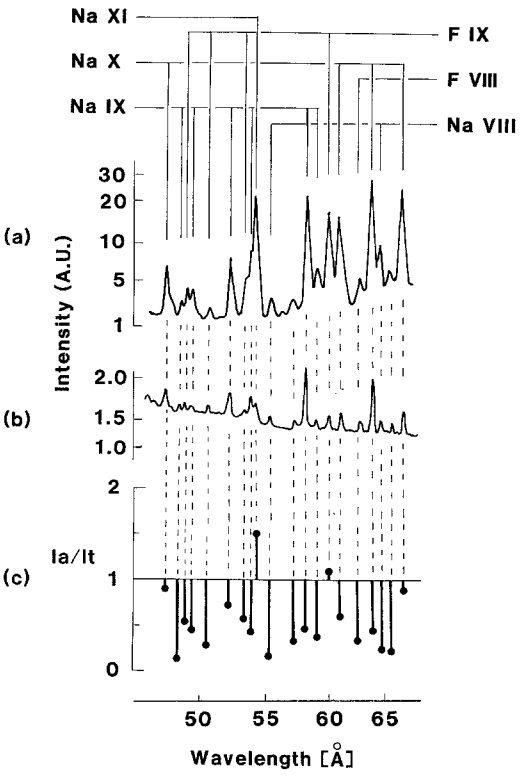

Fig. 6. Densitometer traces of the (a) axial and (b) transverse spectra of an NaF stripe target. Approximate scales linear in intensity are given. The I_a/I_t ratio for each spectral line is shown in (c). Detailed assignments and wavelengths of these lines are given in Table 2

4. Experimental Results

Experimental results on the time-integrated measurements are first presented. Comparing the axial and transverse spectra shown in Fig. 5, we find that the intensities of the Na XI Hα doublet relative to the Na IX $4p^2P$–$2s^2S$ line are stronger in the axial direction. By using the calibration data for the relative sensitivity of the two spectrometers shown in Fig. 3, the actual I_a/I_t ratio is determined for each line and the result is given in Fig. 5c. The Hα doublet have I_a/I_t larger than 1 showing that they have gain, whereas the resonance line of the Li-like Na has $I_a/I_t<1$ showing it has absorption. The $J=5/2$–$3/2$ component of Hα has a higher gain than the $J=3/2$–$1/2$ component as expected. The gL value is determined from the I_a/I_t ratio using (1) and then the gain coefficient g using $L=0.6$ cm. Hereafter we only refer to the gain of the $J=5/2$–$3/2$ component since its gain value has a higher accuracy.

Before discussing in more detail on the gain of Na XI Hα, we examine gain or loss of other transitions. Figure 6 shows densitometer traces of the axial and transverse spectra of a NaF stripe target over 40–70 Å and the I_a/I_t ratios for various spectral lines whose detailed assignments are given in Table 2. The spectral lines belonging to 3–2 transitions in He-like Na ions were assigned with reference to the calculation by Sanders and Knight [38] since it gives good agreement with the spectra that we have recorded on both Na and Mg in comparison to other references [39, 40]. Wavelengths of other lines were taken from the Kelly's table [39]. It should be noted that these spectra are linear in optical density, but not in intensity whose approximate scale is given in each trace. The Na XI Hα has the largest I_a/I_t and exceeds 1. The resonance lines such as C V $2p^1P$–$1s^1S$ at 40.27 Å, Na IX $4p^2P$–$2s^2S$ at 53.86 Å and Na IX $4d^2D$–$2p^2P$ at 58.25 Å have $I_a/I_t<0.5$ showing these lines are optically thick. Some of the lines are optically transparent, i.e. $I_a/I_t\sim1$, such as Na X $4d^3D$–$2p^3P$ at 47.47 Å, Na X $3d^1D$–$2p^1P$ at 66.29 Å, and F IX $4d^2D$–$2p^2P$ at 59.95 Å. Although the $3d$–$2p$ transition in He-like ions was examined as a possible candidate for a short wavelength laser [41] and experimental evidence for gain was reported [42], our experimental results suggest that the gain in He-like ions is smaller than the gain in Hα of hydrogenic ions, at least under the present experimental conditions. This result appears to be consistent with a general expectation that the population inversion density for a particular transition between the 3–2

Table 2. Assignments and axial-to-transverse intensity ratios for various spectral lines. Assignments were determined using the wavelengths given in the references shown in this table. Except for Na XI Hα, the doublet structures or blended lines were not deconvoluted in determining I_a/I_t

Transition		Wavelength [Å]	I_a/I_t	Ref.
C V	$2p^1P^0{}_1$–$1s^1S_0$	40.268	0.10	[39]
Na X	$4d^3D$–$2p^3P^0$	47.466	0.90	[38]
Na X	$4p^1P^0$–$2s^1S$	47.519		[38]
Na IX	$5p^2P^0{}_{3/2}$–$2s^2S_{1/2}$	48.553	0.15	[39]
F IX	$7d^2D_{3/2}$–$2p^2P^0{}_{1/2}$	48.934	0.55	[39]
F IX	$7d^2D_{5/2}$–$2p^2P^0{}_{3/2}$	48.989		[39]
Na IX	$6d^2D_{3/2}$–$2p^2P^0{}_{1/2}$	49.326	0.45	[39]
Na IX	$6d^2D_{5/2}$–$2p^2P^0{}_{3/2}$	49.386		[39]
F IX	$6d^2D_{3/2}$–$2p^2P^0{}_{1/2}$	50.555	0.28	[39]
F IX	$6d^2D_{5/2}$–$2p^2P^0{}_{3/2}$	50.613		[39]
Na IX	$5d^2D_{3/2}$–$2p^2P^0{}_{1/2}$	52.116	0.71	[39]
Na IX	$5d^2D_{5/2}$–$2p^2P^0{}_{3/2}$	52.186		[39]
F IX	$5d^2D_{3/2}$–$2p^2P^0{}_{1/2}$	53.494	0.56	[39]
F IX	$5d^2D_{5/2}$–$2p^2P^0{}_{3/2}$	53.558		[39]
Na IX	$4p^2P^0{}_{3/2}$–$2s^2S_{1/2}$	53.860	0.44	[39]
Na XI	$3d^2D_{3/2}$–$2p^2P^0{}_{1/2}$	54.052	1.13	[39]
Na XI	$3d^2D_{5/2}$–$2p^2P^0{}_{3/2}$	54.194	1.47	[39]
Na VIII	$6d^3D_2$–$2p^3P^0{}_1$	55.345	0.16	[39]
Na VIII	$6d^3D_3$–$2p^3P^0{}_2$	55.396		[39]
Na IX	$4d^2D_{3/2}$–$2p^2P^0{}_{1/2}$	58.201	0.45	[39]
Na IX	$4d^2D_{5/2}$–$2p^2P^0{}_{3/2}$	58.279		[39]
Na IX	$4s^2S_{1/2}$–$2p^2P^0{}_{1/2}$	58.954	0.37	[39]
Na IX	$4s^2S_{1/2}$–$2p^2P^0{}_{3/2}$	59.042		[39]
F IX	$4d^2D_{3/2}$–$2p^2P^0{}_{1/2}$	59.906	1.09	[39]
F IX	$4d^2D_{5/2}$–$2p^2P^0{}_{3/2}$	59.984		[39]
Na X	$3p^3P^0$–$2s^3S$	60.682	0.60	[38]
F VIII	$6p^1P^0$–$2s^1S$	62.536	0.31	[39]
F VIII	$6d^3D$–$2p^3P^0$	62.561		[39]
Na X	$3p^1P^0$–$2s^1S$	63.575	0.43	[40]
Na X	$3d^3D$–$2p^3P^0$	63.577		[38]
Na VIII	$4d^3D_2$–$2p^3P^0{}_1$	64.237	0.22	[39]
Na VIII	$4d^3D_3$–$2p^3P^0{}_2$	64.302		[39]
Na X	$3d^1D$–$2p^1P^0$	66.288	0.85	[38]

levels in He-like ions will be lower compared with that for the $3d$–$2p$ transition in hydrogenic ions due to splitting of the energy levels into singlet and triplet terms in He-like ions.

The I_a/I_t ratio for the Na XI Hα $J=5/2$–$3/2$ line obtained in this experiment is larger than 1 but not by much. Therefore careful examination on the measurement accuracy is necessary in order to evaluate the significance of the result obtained in this work. The errors arising from several major factors are evaluated in the following.

(1) The error in the response curve shown in Fig. 4 is 20% at 0.3 D and less at higher optical densities. This error is not directly transferred to the result because the same curve is used for determining the axial-to-transverse intensity ratio and analyses were made to the spectral lines having $0.3<D<1$. The error arising from the film response curve to the intensity ratio is estimated to be within 15%.

(2) The measurement data on the relative sensitivity of the two spectrometers shown in Fig. 3 can be fitted to an empirical curve shown in the figure with an error of within 10%. However the actual error arising from this cross calibration is estimated to be approximately 20% which is the value derived from an experiment made independently where more calibration data were taken in a similar way.

(3) The line shape analysis in Fig. 5 shows that the amount of mixing of nearby lines to the Na XI Hα 5/2–3/2 line is approximately 20% and these fractions have been subtracted from both axial and transverse spectra. Therefore the error arising from this mixing is less than 10%. A larger error arises from imperfect fitting of the convoluted lineshape to the experimental line shape which is ~5% for the axial spectrum and 15% for the transverse spectrum.

Since these errors are independent of each other, the total error in determining I_a/I_t ratio is given by root-mean-square of these errors. Therefore the error in I_a/I_t is estimated to be approximately $\pm 30\%$.

The dependence of gain on target structure and irradiation energy was studied in this experiment. Results are summarized in Table 3. The determination of gain on a fiber target was not successful due to the weak spectral intensity available from this target. The gain coefficient on Na XI Hα obtained in this measurement with the stripe and foil targets was approximately 1 cm^{-1}. Although this is a small value considering together with a fairly large error accompanied with this value, a positive gain on Na XI Hα has been consis-

Table 3. Measured time-integrated gain coefficients of the Na XI Hα $J=5/2$–$3/2$ transition for different irradiation conditions

Target	Laser Energy [J]	I_a/I_t	g [cm^{-1}]
NaF Stripe	73	1.33 ± 0.40	$0.9^{+0.8}_{-1.2}$
NaF Stripe	153	1.12 ± 0.34	$0.4^{+0.8}_{-1.3}$
NaF Foil	63	1.47 ± 0.44	$1.2^{+0.8}_{-1.1}$
$Na_2B_4O_7$ Stripe	69	0.74 ± 0.22	$-1.1^{+0.9}_{-1.4}$

tently obtained when the target was irradiated in similar irradiation conditions as shown in Table 3. It should be noted that this result was obtained in both space- and time-integrated measurement. According to our numerical analysis on a different but similar experiment, each of space- and time-averaging reduces gain by a factor of 2 or more, depending on the irradiation conditions. Therefore it is inferred that approximately 4 cm^{-1} or higher gain may be attained local in space and time in the present measurement. The result of the time-resolved measurement is given later in this section.

Several interesting observations can be made from Table 3. First the diluted $Na_2B_4O_7$ stripe target definitely shows smaller I_a/I_t compared with the NaF stripe target. This will be reasonable if the Lα trapping is not quenching the gain, since the Na fraction is ~1/6 in the diluted target. The observed gain is not very sensitive to the target structure, i.e. between the stripe and the foil. Since spatial averaging will lead to a lower gain for the foil target in a space-integrated measurement due to existence of larger volume of non-amplifying region as was discussed by Eder et al. [30], the result in Table 3 might indicate attainment of a larger localized gain with the foil target than with the stripe target. The gain in the stripe target does not appear to be strongly dependent on the irradiation laser energy above 70 J. This may arise for the following reason. The stripe thickness of 1 μm is larger than the calculated ablation depth of 0.5 μm. Therefore the whole body of NaF is not completely heated and the gain region is produced in an expanding plasma during cooling period after laser heating. When the irradiation intensity exceeds the intensity required to ionize Na atoms to the fully-stripped state at the surface of the target, there always exists an optimum plasma region, at a certain initial depth from the surface, in which population inversion is generated. The effect of increasing the intensity is to increase the non-amplifying plasma region which reduces the gain in space- and time-integrated measurement. Since the results obtained here are preliminary, more detailed experimental and theoretical investigations will be necessary for optimizing the target structure and irradiation conditions.

Temporal evolution of the gain was also measured with the streak cameras attached to the axial and transverse spectrometers. Relative sensitivity of the two instruments was calibrated as described in the previous section. Figure 7 shows a streaked axial spectrum of a NaF stripe target irradiated at a 148 J laser energy. The Na XI Hα emission starts at the rising portion of the laser pulse, becomes maximum at ~170 ps after the laser peak, and decays initially rapidly reaching to half intensity at ~300 ps after the

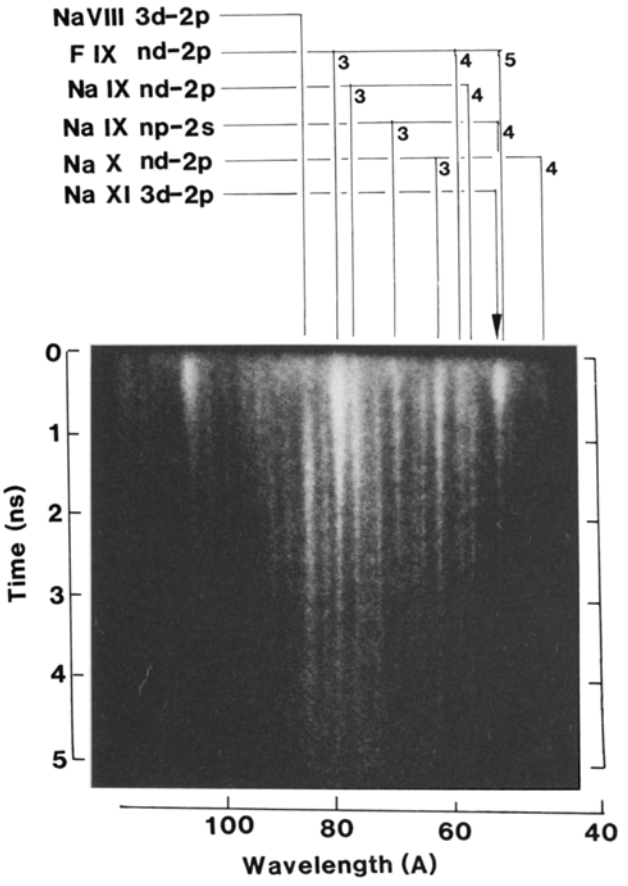

Fig. 7. Streak camera record of the axial emission of a NaF stripe target. The time origin is at the peak of the laser pulse. The Na XI Hα line is shown by an arrow

maximum emission, and then decays more slowly afterwards. In contrast the emission due to He-like, Li-like, and Be-like Na ions last longer. With the streak camera measurement, we can not resolve the Hα doublet and also the lines which are adjacent to Na XI Hα shown in Fig. 5. The contribution of these adjacent lines to the observed time dependence of the Na XI Hα emission was evaluated and subtracted as follows. The total energy of each of these adjacent lines relative to Hα is known from the time-integrated data. The time dependence of each line was assumed to be the same as that of the line belonging to the same (or similar) sequence and is not overlapped with other transitions in the streak spectrum: that is, Na IX $4d$–$2p$ at 58 Å for Na IX $4p$–$2s$ and F IX $4d$–$2p$ at 60 Å for F IX $5d$–$2p$. Since emission of these lines starts slowly after laser irradiation and becomes maximum 200–300 ps after the maximum emission of Na XI Hα, these lines contribute mainly to the decaying part of the Na XI Hα emission, particularly after decaying to half the maximum intensity.

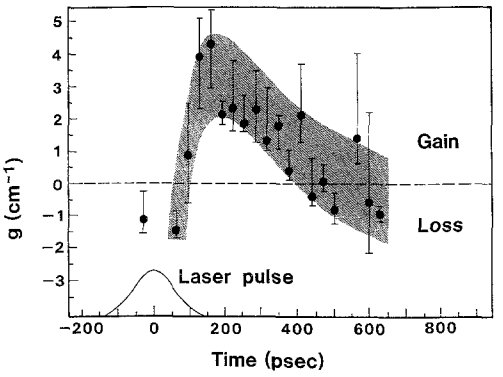

Fig. 8. Time-resolved gain of the Na XI Hα line for a NaF stripe target with 148 J laser irradiation

The time dependence of the gain coefficient $g(t)$ was determined from $I_a(t)/I_t(t) = \{\exp[g(t)L] - 1\}/[g(t)L]$ where $I_a(t)$ and $I_t(t)$ are time-dependent axial and transverse Hα intensities. The result is shown in Fig. 8. The gain starts ~100 ps after the laser peak, becomes maximum at 150–200 ps and decays gradually as the Hα emission intensity decreases. The error bars in this data arise from granular noises of the image intensifier of the streak camera attached to the transverse spectrometer and the larger error bars after ~600 ps were caused by an accidental electrical noise in this streak tube. Regarding the accuracy of this result, the intensities of the B V $2p$–$1s$ line at 48.6 Å detected with the two streak cameras and used for cross calibration were sufficiently strong and the wave forms of their time dependences agreed with each other very well, confirming the reliability of the calibration data on the intensity responses of the two streak cameras. The error arising from transfering the calibration data from 48.6 Å to 54.2 Å for Na XI Hα is evaluated to be approximately 10% since the changes in spectral responses of the photocathodes are less than 10% and the spectral dependence of the relative sensitivity of the two spectrometers have been reliably calibrated in time-integrated measurement. Therefore the error in $I_a(t)/I_t(t)$ at the peak gain will be well within ±30% which corresponds to the error in the maximum gain of $g = 3.2 \pm 1.0\,\mathrm{cm}^{-1}$. Considering the reduction of gain in time-averaging, this peak gain is consistent with and more accurate than the time-integrated gain of $g = 0.4^{+0.8}_{-1.3}\,\mathrm{cm}^{-1}$ obtained at a similar irradiation condition and shown in Table 3. From the results of the time-integrated and time-resolved measurements, we conclude that gain on Na XI Hα has been observed.

5. Summary

We have presented time-integrated and time-resolved measurements of gain on Na XI Hα at 54.2 Å. Planar stripe or foil targets coated with either NaF or $Na_2B_4O_7$ were irradiated with 351 nm laser light. With NaF targets, gain coefficient of $1.2^{+0.8}_{-1.1}\,\mathrm{cm}^{-1}$ in time-integrated measurement and $3.2 \pm 1.0\,\mathrm{cm}^{-1}$ in time-resolved measurement was obtained. Gain on Na XI Hα was not observed with the $Na_2B_4O_7$ target, indicating that gain quenching by Lα trapping is not a strong effect. Our experimental results do not show gain in $3d$–$2p$ transitions in He-like Na.

A qualitative account of the present experimental results has been presented previously based on a simple steady-state atomic physics model and a two-dimensional hydrodynamic simulation [21]. More quantitative analyses based on a detailed atomic physics model coupled to a 2D hydrodynamic code will be presented in a later publication, in which evaluation of ionization balance and plasma parameters inferred from spectroscopic data will be included.

Finally we note that in the present experiment, gain on Mg XII Hα at 45.5 Å was also measured and a time-integrated gain larger than the value for Na XI Hα was obtained. In addition, in our recent experiment where a target was irradiated with a laser pulse of the shorter duration of 28 ps, an approximately 3 times higher gain was obtained on Na XI Hα with a smaller laser energy [43]. These results suggest that it will be possible to achieve significant gain at the wavelengths near to, and possibly within, the water window when the irradiation conditions are optimized.

Acknowledgements. This work was performed as a joint research between the Institute of Laser Engineering, Osaka University and the Central Laser Facility, Rutherford Appleton Laboratory. We are grateful for a variety of support offered by the staff at these laboratories. Financial support by the Japan Society for the Promotion of Science to M. H. Key and P. R. Herman and by the Inoue Foundation for Science to P. R. Herman is gratefully acknowledged. This work was supported partly by a Grant-in-Aid for Scientific Researches by Monbusho, contract no. 62302021.

References

1. M.D. Rosen, P.L. Hagelstein, D.L. Matthews, E.M. Campbell, A.U. Hazi, B.L. Whitten, B. MacGowan, R.E. Turner, R.W. Lee, G. Charatis, G.E. Bush, C.L. Shepard, P.D. Rockett: Phys. Rev. Lett. **54**, 106 (1985)
2. D.L. Matthews, P.L. Hagelstein, M.D. Rosen, M.J. Eckart, N.H. Ceglio, A.U.Hazi, H. Medecki, B.J. MacGowan, J.E. Trebes, B.L. Whitten, E.M. Campbell, C.W. Hatcher, A.M. Hawryluk, R.L. Kauffman, L.D. Pleasance, G. Rambach, I.H. Scofield, G. Stone, T.A. Weaver: Phys. Rev. Lett. **54**, 110 (1985)
3. B.J. MacGowan, M.D. Rosen, M.J. Eckart, P.L. Hagelstein, D.L. Matthews, D.G. Nilson, T.W. Phillips, J.H. Scofield, G. Shimkaveg, J.E. Trebes, R.S. Walling, B.L. Whitten, J.G. Woodworth: J. Appl. Phys. **61**, 5243 (1987)

4. B.J. MacGowan, S. Maxon, P.L. Hagelstein, C.J. Keane, R.A. London, D.L. Matthews, M.D. Rosen, J.H. Scofield, D.A. Whelan: Phys. Rev. Lett. **59**, 2157 (1987)
5. B.J. MacGowan, S. Maxon, C.J. Keane, R.A. London, D.L. Matthews, D.A. Whelan: J. Opt. Soc. Am. B **5**, 1858 (1988)
6. T.N. Lee, E.A. McLean, R.C. Elton: Phys. Rev. Lett. **59**, 1185 (1987)
7. S. Suckewer, C.H. Skinner, H. Milchberg, C. Keane, D. Voorhees: Phys. Rev. Lett. **55**, 1753 (1985)
8. D. Jacoby, G.J. Pert, S.A. Ramsden, L.D. Shorrock, G.J. Tallents: Opt. Commun. **37**, 193 (1981)
9. C. Chenais-Popovics, R. Corbett, C.J. Hooker, M.H. Key, G.P. Kiehn, C.L.S. Lewis, G.J. Pert, C. Regan, S.J. Rose, S. Sadaat, R. Smith, T. Tomie, O. Willi: Phys. Rev. Lett. **59**, 2161 (1987)
10. G.P. Kiehn, J. Edwards, R.A. Smith, O. Willi, C.L.S. Lewis, D. O'Neill, C. Regan, G. Pert, S. Ramsden, M. Grande, M.H. Key, S.J. Rose, A. Carillon, M. Guennou, P. Jaegle, G. Jamelot, A. Klisnick, A. Sureau: SPIE **831**, 270 (1987)
11. J.F. Seely, C.M. Brown, U. Feldman, M. Richardson, B. Yaakobi, W.E. Behring: Opt. Commun. **54**, 289 (1985)
12. Y. Kato, P.R. Herman, T. Tachi, K. Shihoyama, K. Kamei, H. Shiraga: SPIE **831**, 299 (1987)
13. D.L. Matthews, E.M. Campbell, K. Estabrook, W. Hatcher, R.L. Kauffman, R.W. Lee, C.L. Wang: Appl. Phys. Lett. **45**, 226 (1984)
14. P.R. Herman, T. Tachi, K. Shihoyama, H. Shiraga, Y. Kato: IEEE Trans. Plasma Sci. **16**, 520 (1988)
15. P. Jaegle, G. Jamelot, A. Carillon, A. Klisnick, A. Sureau, H. Guennou: J. Opt. Soc. Am. B **4**, 563 (1987)
16. T. Hara, K. Ando, N. Kusakabe, H. Yashiro, Y. Aoyagi: Jpn. J. Appl. Phys. **28**, L-1010 (1989)
17. D. Kim, C.H. Skinner, A. Wouters, E. Valeo, D. Voorhees, S. Suckewer: J. Opt. Soc. Am. B **6**, 115 (1989)
18. R.A. London, M.D. Rosen, J.E. Trebes: Appl. Opt. **28**, 3397 (1989)
19. S. Maxon, S. Dalhed, P.L. Hagelstein, R.A. London, B.J. MacGowan, M.D. Rosen, G. Charatis, G. Busch: Phys. Rev. Lett. **63**, 236 (1989)
20. Y. Kato, M. Yamanaka, H. Daido, T. Tachi, H. Nishimura, H. Shiraga, E. Miura, P.R. Herman, H. Takabe, T. Jitsuno, M. Takagi, S. Nakai, C. Yamanaka, M.H. Key, G.J. Tallents, S.J. Rose: *OSA Proc. Short Wavelength Coherent Radiation: Generation and Applications*, Vol. **2** (Opt. Soc. Am., Washington, DC 1988) pp. 47–51
21. H. Nishimura, H. Shiraga, H. Daido, T. Tachi, P.R. Herman, E. Miura, H. Takabe, M. Yamanaka, Y. Kato, G.J. Tallents, M.H. Key: *OSA Proc. Short Wavelength Coherent Radiation: Generation and Applications*, Vol. **20** (Opt. Soc. Am., Washington, DC 1988) pp. 137–140
22. G.J. Pert: J. Phys. B **9**, 3301 (1976)
23. G.J. Pert: J. Phys. B **12**, 2067 (1979)
24. G.J. Pert: Plasma Phys. Cont. Fusion **27**, 1427 (1985)
25. G.J. Pert: J. Opt. Soc. Am. B **4**, 602 (1987)
26. R.W. McWhirter, A.G. Hearn: Proc. Phys. Soc. **82**, 641 (1963)
27. M.H. Key: Rutherford Lab. Rep. **RAL-87-041**, 100 (1987)
28. J.P. Apruzese, J. Davis, P.C. Kepple, M. Blaha: J. Phys., Suppl. Colloque C **6**, C6–15 (1986)
29. A.K. Davé, G.J. Pert: J. Phys. B **17**, 4953 (1984)
30. D.C. Eder, M.D. Rosen, R.W. Lee, J.E. Trebes, N.M. Ceglio, M.J. Eckart, R.L. Kauffman, B.J. MacGowan, D.L. Matthews: J. Opt. Soc. Am. B **4**, 1949 (1987)
31. G.J. Pert, S.J. Rose: Appl. Phys. B **50**, 307 (1989)
32. I.N. Ross, J. Boon, R. Corbett, A. Damerell, P. Gottfeldt, C. Hooker, M.H. Key, G. Kiehn, C. Lewis, O. Willi: Appl. Opt. **26**, 1584 (1987)
33. T. Harada, T. Kita: Appl. Opt. **19**, 3987 (1980)
34. B.L. Henke, J.P. Knauer, K. Premarate: J. Appl. Phys. **52**, 1509 (1981)
35. B.L. Henke, S.L. Kwok, J.Y. Uejio, H.T. Yamada, G.C. Young: J. Opt. Soc. Am. B **1**, 818 (1984)
36. B.L. Henke, F.G. Fujiwara, M.A. Tester, C.H. Dittmore, M.A. Palmer: J. Opt. Soc. Am. B **1**, 828 (1984)
37. K. Eidman, T. Kishimoto, P. Herrmann, J. Mizui, R. Pakula, R. Sigel, S. Witkowski: Laser and Particle Beams **4**, 521 (1986)
38. F.C. Sanders, R.E. Knight: Phys. Rev. A **27**, 1279 (1983)
39. R.L. Kelly: J. Phys. Chem. Ref. Data **16** (Suppl.) No. 1–3 (1987)
40. S. Bashkin, J.O. Stoner, Jr.: *Atomic Energy Levels and Grotrian Diagrams*, Vol. **1** (North Holland, Amsterdam 1975)
41. J.P. Apruzese, P.C. Kepple, J. Davis, J. Pender: IEEE Trans. Plasma Sci. **16**, 529 (1988)
42. H. Kuroda, K. Muroo, K. Naito, Y. Tanaka: Tech. Rept. ISSP, Univ. Tokyo, Ser. A No. 1955 (1988)
43. Y. Kato, H. Azuma, K. Yamakawa, H. Takabe, T. Tachi, T. Nishio, S.A. Ramsden, S.J. Rose: 19th Anomalous Absorption Conf., Durango, Colorado, June 19–23, 1989 (unpublished)